Controllable continuous-wave dual-wavelength operation of in-band diode-pumped Nd:$GdVO_4$/Nd:YVO_4 composite laser

By

Chinedu Desmond-Patrick Onyenekwu

A Thesis submitted to the Faculty of Graduate Studies of

The University of Manitoba

In partial fulfillment of the requirements of the degree of

MASTER OF SCIENCE

Department of Electrical and Computer Engineering

University of Manitoba

Winnipeg

Abstract

This thesis presents a controllable continuous-wave dual-wavelength diode-pumped laser based on a composite Nd:$GdVO_4$/Nd:YVO_4 crystal. Controllability for the pair of spectral output was achieved by changing the operating temperature of the fiber-coupled laser diode pump using a digital temperature controller. The resulting temperature-dictated pumping wavelength provided a precise and turnkey means of intensity control for the two emitted spectral lines as either line showed strong and proportionate intensity change in response to the wavelength of excitation by the pump. The intensity ratio for the pair was in favor of the $GdVO_4$ emission at 1063 nm while pumping at about 912 nm while the YVO_4 emission was relatively lower and vice versa while pumping at 914 nm. For power scalability, a low-quantum defect (QD) approach was adopted using in-band pumping. This was specifically performed around the 910 - 914 nm wavelength range considering and corresponding to the longer Nd:$GdVO_4$/Nd:YVO_4 absorption bands. Using this efficiency-increasing initiative, the laser produced a maximum output power of 4.48 W with 11.55 W of absorbed power, corresponding to a slope and optical-to-optical efficiency of 43.8 % and 38.8 % respectively. These parameters are notably the highest ever reported compared to all previous works using a similar composite crystal for dual wavelength operation.

Acknowledgement

I would like to express my profound gratitude to Prof. Arkady Major for his patience and guidance throughout my graduate study and research in the Biomedical and Laser Photonics group of the department. I am grateful for the knowledge I acquired through his unwavering support and direction.

I acknowledge the contributions of the past and present students of the research group particularly: Reza, Sujith, Shirin, Mohammad, Anisur, Chandan, Zohreh, Rubel. I gained a lot from the formal and informal exchange and presentations. I am particularly grateful to Mohammad Nadimi for generously according me full co-operation - time, knowledge and experience. His practical assistance in setting up and troubleshooting the laser helped for a smooth take-off in the laboratory; the continued sharing and technical support were invaluable toward the overall success of this research.

I also appreciate the contribution of the students and faculty - for all the information and exposure I received during the program. Prof. Cyrus Shafai, Bernice, Keverley and Amy to mention just a few. Special thanks to the members of my examining committee - Dr. G. Bridges and Dr. J. Burgess, especially for their time and feedback.

To my loving parents Theo and Vicky, siblings and friends, the Onyenekwus, Anyaokus, Amobis, Nwankwos, Egbufors, Michelle and Gilles Marchildon, Paulette and Gerry Hughes, Fr. Armand Le Gal: thank you all! Lastly, my heartfelt appreciation goes to my immediate family especially my wife Nneka – I am grateful for your love and encouragement; my youngsters – Kenny and Somie – for everything we missed out on.

My time in the university was simply rewarding. To God be the glory!

Table of Contents

Abstract i

Acknowledgement ii

List of Figures v

List of Tables vii

List of symbols and abbreviations viii

Chapter 1 1

1.1 Introduction 1

1.2 Motivation 5

1.3 Objectives 9

1.4 Contributions 10

1.5 Thesis outline 11

Chapter 2 - Theoretical Overview 13

2.1 Dual-wavelength lasers 13

2.2 Low Quantum Defect (QD) Pumping 15

2.3 Highlight of the Crystal Used 20

2.3.1 $Nd:YVO_4$ 22

2.3.2 $Nd:GdVO_4$ 23

2.4 Previous records of DW $Nd:GdVO_4$ /$Nd:YVO_4$ lasers 24

Chapter 3 - Experimental setup and Results 27

3.1 Crystal specification and setup 27

3.2 Laser diode pump 29

3.3 Cavity modeling and design 31

3.4 Results and discussion 36

Chapter 4 - Conclusion and future work 43

References 46

Appendix A – Gaussian Beams and the ABCD Law 50

List of Figures

Figure 2.1 A pair of DW spectral lines 13

Figure 2.2 Low QD initiative by in-band pumping (into the upper laser band). Δ graphically illustrates the transition that leads to heat generation - now eliminated by pumping directly into the laser band using this technique 15

Figure 2.3 Quantum defect illustration for a 4-level laser. E_P and E_L depict the energy of the pump and laser respectively. E_1: Ground state, E_2: Lower laser level, E_3: Upper laser or metastable level, E_4: Pump or highly excited band. [© R. C. Talukder 2016] [21] 17

Figure 2.4 Schematic of pump and laser energy transitions with corresponding wavelengths for Nd:$GdVO_4$ (left) and Nd:YVO_4 (right) [© M. Nadimi 2018] 18

Figure 2.5 Above: absorption spectra for Nd: $GdVO_4$ [21]. The blue arrows (inset) highlight absorption 'bump' in the spectra around 912 nm. This was explored for the long wavelength pumping 21

Figure 2.6 Below: absorption spectra for Nd:YVO_4 [20]. Blue arrows (inset) highlight absorption 'bump' in the spectra around 914 nm. This was explored for the long wavelength pumping 21

Figure 3.1 Color-coded schematic showing composite crystal geometry and direction of pumping.. 27

Figure 3.2 Crystal cooling arrangement. Indium foil-wrapped-crystal is sandwiched in metal holder 28

Figure 3.3 Recirculating water chiller of the cooling system for laser. Digital displays show both the room temperature (to the left) and the temperature of the water in the cooling system (to the right) as at time of photo 28

Figure 3.4 Laser diode cooling setup with temperature control 29

Figure 3.5 Plot of shifting peak wavelength for the laser diode due to temperature variation 31

Figure 3.6 reZonator-generated schematic of the modeled DW laser cavity 32

Figure 3.7 Screenshot of reZonator showing the changing beam radius of the laser propagating in the cavity 33

Figure 3.8 Schematic of the experimental laser setup 35

Figure 3.9 Photograph of the actual laser cavity setup. Red dashed line shows intracavity laser beam path 35

Figure 3.10 Dual-wavelength output power versus the absorbed pump power (Temp. 30 ºC) 36

Figure 3.11 Laser beam quality measurement at full output power and the output beam shape (inset) 39

Figure 3.12 Laser diode spectra at 29 °C, 36 °C and 39 °C.....40

Figure 3.13 Dual-wavelength operation spectra at circa 1063 and 1064 nm. (a) - (c) Control of the power ratio between the two lasing wavelengths achieved by temperature-determined peak pumping wavelength of the laser diode. (a) λ_{LD} = 911.3 nm (T_{LD} = 30 ºC), (b) λ_{LD} = 912.5 nm (T_{LD} = 33 ºC) and (c) λ_{LD} = 913.3 nm (T_{LD} = 36 ºC). Where T_{LD} = is the operating temperature of the laser diode 41

Figure 3.14 Normalized laser intensity at 1063 and 1064 nm as a function of the laser diode peak wavelength 42

List of Tables

Table 2.1 Properties for both vanadates for the 1063/1064 nm laser transition (considered for 0.3 at.% and 0.5 at.% for Nd:YVO_4 and Nd:$GdVO_4$ respectively)[5]……24

Table 2.2 Performance summary for some previous DW lasers using composite crystals……...26

List of symbols and abbreviations

Symbol	Denotation
T	Florescence or upper state lifetime
E_P	Energy of pump
E_L	Energy of laser
σ_{em}	Emission cross section
$\Delta\lambda$	Gain bandwidth
η_F	Fractional thermal loading
λ_P	Pump wavelength
λ_L	Laser wavelength
k_c	Thermal conductivity
M^2	Beam quality factor
w_P	Pump radius
Abbreviation	**Meaning**
CW	Continuous-wave
DW	Dual-wavelength
QD	Quantum defect
DFG	Difference Frequency Generation
NA	Numerical aperture
OC	Output coupler
DM	Dichroic mirror
HT	High transmission
HR	Highly reflective
LD	Laser diode
RoC	Radius of curvature
FWHM	Full-width at half maximum

Chapter 1

1.1 Introduction

The first laser was developed in 1960 by T. H. Maiman following the formulation of the original principles and theory of laser operation reported by C. H. Townes and A. L. Schawlow in 1958 [1]. In those fledgling days, lasers were ironically taunted as solution seeking a problem [2]. Soon after the introduction of the first laser which was a flash-lamp-pumped ruby crystal, other lasers were developed making use of a variety of materials such as gases and semi-conductor materials. Through the years, improvements in their design and operation especially in their means of excitation and the laser materials, has led to the development of numerous types of lasers. Some of these lasers deliver single or multi-wavelength radiation across the continuous-wave (CW) and pulsed regimes (such as the Q-switched and mode-locked lasers). It is noteworthy to highlight that in the CW type, there is continuous output of the laser radiation. However, laser action is sustained only for brief periods in the pulsed version.

A laser basically comprises of three main components: (i) a material (solid, liquid, gas) in which energy can be stored (otherwise called a gain medium), (ii) a mechanism of excitation that is the source of energy that is absorbed and (iii) a means of providing positive feedback known as the resonator or optical cavity in which light oscillates in continued round trips to ensure sustenance of the stimulated emission producing the lasing. The laser output is released in part from the cavity through a partially reflecting mirror - one physical boundary of the optical resonator or cavity.

In order to achieve laser operation, the material or gain medium is placed within the cavity while the spectrally-matched excitation mechanism, otherwise called an optical pump source, is used to excite this material causing electronic transitions from the ground state to a higher energy level. The cavity -

which may essentially be a two-mirror arrangement with one totally reflecting and the other partially reflecting, simultaneously ensures positive feedback by containment of the process as well as allows partial release of light output as mentioned above. The pumping causes electrons of the material which are normally in thermal equilibrium to go into excited state. That is, from the ground state to a higher energy state. Consequently, a rising number of excited or upper state electrons results in a population inversion – described in terms of the upper state population relative to that of the ground state.

The aforementioned process progresses and subsequently yields photon emission which initially proceeds spontaneously with random wavelengths. Beyond a given threshold pump power, this random process progressively reaches a stimulated regime from the interaction of a spontaneously emitted photon interacting with an excited electron. The stimulated emission continues in a geometric progression as the round trip gain from the laser material now exceeds the passive losses of the cavity. From that point when the threshold is surpassed, further increase in the pump power contributes towards increasing the laser output power. Also in this regime, the stimulated emission of photons proceeds and it is not only sustained within the cavity but it is multiplied by each emitted photon yielding two others per interaction with the excited electrons.

Hence for a laser using a basic 2-mirror cavity:

$$G = R1R2e^{2(\gamma-\alpha)L} \tag{1.1}$$

Where,

G = round trip gain

$R1, R2$ = reflectivity of cavity mirrors

γ = effective gain coefficient

α = effective loss coefficient

L = cavity length

Based on the nature of the stimulated emissions, the yielded photons have properties that are identical such as their wavelength, direction, phase and polarization. Thus lasers inherently possess unique properties on account of their mechanism of operation. Among these characteristics, they normally produce beams that are coherent, monochromatic and also highly radiant. Their coherence refers to the property of each of the emitted photons whereby they are approximately in phase with respect to each other. On the other hand, laser beams are also monochromatic since photons are emitted with the same energy and consequently wavelength. Their brightness results mainly from the spatial nature of the beam which is usually very narrow and highly directional.

The solid-state type of lasers which are based on gain media of either metal-ion doped crystals or glasses are very popular and rely on optical pumping for excitation mechanism particularly using laser diode pumps. Diode-pumped solid-state lasers are especially known for benefits such as their extended lifetime, compactness, excellent beam quality as well as their higher efficiency [1]. Quite often, a laser is described in terms of the radiation focused onto the laser material from the excitation source or pump or on other hand, the radiation which is circulating in the cavity. These are tagged the pump modes and the resonator or laser modes respectively. The latter forms frequency-specific standing wave patterns within the cavity. The modes may be described in terms of their spectral or temporal characteristics - frequency, power, phase and polarization.

Lasers notably emit very bright light that is highly intense and directional; their radiation is typically of the same wavelength. Since laser beams are highly collimated and laser radiation is coherent, they can be focused onto a very tiny area for a variety of purposes. Lasers and laser-enabled devices presently find use in more areas of science and technology than was previously imagined in their infancy days owing to combination of not only their properties and characteristics but also advances in laser materials used [2]. They particularly find utility and applications in the biomedical, chemical,

mechanical, and industrial sectors among others [1 - 3]. In the listed areas, their applications include but are not limited to their use as biomedical or industrial sources for radiation generation in different types of imaging, material identification; also for ablation and deposition, differentiation and irradiation to mention just a few [4].

Lasers are also used to facilitate research and development across the ever-broadening technology space as well as the constantly evolving challenges usually encountered with it. They currently provide original solutions or in some other cases, they offer highly improved and effective alternatives to previously existing ones as in the case of higher resolution and more efficient laser-based projectors. Also in medicine, the critical demands of extreme caution as well as high success rate requirement for eye surgeries are jointly met in the newer laser-driven procedures. The numerous benefits of speed, precision and accuracy afforded by their dependence on lasers are at the core of their increasing popularity and availability.

Lasers unarguably drive tools and techniques used in broadly scalable engineering processes delivering increased throughput and effectiveness. These span across the miniature design and laser-assisted microfabrication processes for microelectronic production up to the industrial scale laser cutting, drilling and welding, peening – with broad application and utility in the maritime, automobile and aircraft industries to mention a few.

Ongoing academic and industry collaboration seek ways to increase their capabilities and performance as well as target their power and efficiency (operational) limitations for alleviation or mitigation [3]. Thus providing more versatile lasers with superior performance offering increased compactness and simplicity, reliability and stability, efficiency and operational effectiveness [3, 4]. These pleasant though initially unforeseen turn of events in laser developments and its applications have ultimately aided the reversal of that original notion of no-utility as more areas of human endeavor and applications

currently seek lasers [2]. Hence, based on their extensive reach and importance, nearly six decades after the first laser was developed, lasers are still subject of further research and development yielding variants with wider ranging capabilities and diverse potentials [4]. For instance, remote sensing using laser may require more than one laser since often times, more than a single wavelength radiation is needed. However, since conventional lasers produce radiation at just one output wavelength, hence there is a need for the development of different types of multi-wavelength lasers [2].

1.2 Motivation

CW dual-wavelength (DW) solid-state lasers are a more recent and relatively less common type of solid-state lasers [1]. They are useful in the fields of spectroscopy, instrumentation, remote sensing, and biomedicine among others [1 - 4]. In biomedicine for example, they may be used for cytometry. They are also very promising for stable terahertz (THz) frequency generation [5]. The benefits of terahertz radiation are discussed in greater detail in the next chapter.

As introduced earlier, DW lasers offer multipurpose capability in a single laser device with their dual-wavelength radiation [3]. This provides an edge of compactness and versatility over the conventional lasers which generates radiation at a single wavelength [2]. DW lasers have been reported and practically demonstrated with a variety of gain media using laser host materials that are singly doped like Nd:YVO_4, Nd:$GdVO_4$, Nd:YAG, Nd:YLF; as well as some other co-doped single material gain media [2, 4]. Other implementations include hybrid configurations, in which two different gain media are placed in close proximity within a single resonator or laser cavity [5].

The various implementations using Nd doping leverage well-known benefits of using neodymium as active ions. For instance, neodymium (Nd^{3+}) doped crystals are notably better for obtaining relatively higher power compared to the other four-level laser materials [1, 4]. The Nd^{3+} ions favor a group of energy level transitions that is slightly modified by the crystal fields of the host material as a result of

its interaction with the Nd^{3+} ions [1]. Out of the three main transitions allowed in Nd^{3+} doped vanadates (i.e. Nd:YVO_4, Nd:$GdVO_4$) which occur at 0.9 μm, 1.06 μm and 1.3 μm, the transition around 1.06 μm is known to have the highest stimulated emission cross-section [1, 4 - 7]. In this work, using a bonded Nd:YVO_4,/Nd:$GdVO_4$ composite crystal, the DW operation is based on transitions from the $^4F_{3/2}$ to $^4I_{11/2}$ manifolds providing a pair of spectral output lines at the peak emission cross-sections around 1063/1064 nm [4 - 6].

DW lasers, like the conventional lasers, also endure performance setbacks in operation [3, 5]. The more prevalent ones are due to performance degradation and complications resulting from thermal loading in the crystal. Other issues include such operational challenges as may be presented by intense competition for gain by the multi-frequency radiation for lasers with more than one emission line. This situation arises from the fact that typically in DW lasers both spectral lines originate from the same gain medium and therefore they contest for amplification. Essentially, the line with greater net gain will grow stronger saturating the gain while the competing line experiences the opposite evidenced by power and performance degradation [8]. The dynamics of this competition inadvertently leads to power instability in the laser directly limiting the ability to independently control the power intensity ratio for the pair of output of the DW laser [5, 8]. This in turn inevitably restricts areas of applications for these type of lasers [3 – 5]. Thus, in some of the highlighted implementations, DW power-tuning optical components were introduced to enable the tuning of the DW radiation power intensity ratio. These components include mirrors with special coatings and various designs of output couplers, gratings and etalons [4].

Furthermore, on account of quantum defect (QD) heating arising from thermal loading of the crystal host material due to the energy difference between the pump photons and those of the laser [7, 9], the greater the difference between the pump and laser radiation wavelengths, the more the fractional

thermal loading due to non-radiative transitions [1]. Consequently, pumping the Nd:doped vanadates around the traditional 808 nm wavelength, inevitably exposes the laser crystal to an increased tendency for more severe thermal issues from the correspondingly larger contribution of quantum defect heating at the shorter pump wavelength relative to when pumped at a longer absorption-feasible wavelength that is closer to the lasing wavelength [9].

QD heating typically leads to thermal lensing as a heat gradient develops across the crystal cross section [7 - 10]. This progressively distorts the laser crystal and laser beam output. If uncontrolled, it produces significant mechanical stress that ultimately results in crystal fracture beyond particular material limits [9, 10]. Indeed, susceptibility to the highlighted limitations among others adversely affect not just the ability to scale the laser power output [11, 12], but also the controllability of the DW intensity ratios.

To mitigate the issue with gain competition, an original composite crystal of Nd:YVO_4 and Nd:$GdVO_4$ that is diffusion-bonded was recently designed for DW operation [3]. Using two variants of this composite crystal, new initiatives for controlling the intensity ratios of the pair of spectral radiation were also experimentally demonstrated [15, 16, 17]. They were based on the lateral variation of pumping radiation using a flat vertical interface diffusion-bonded crystal in one case and for the other, using a wedged interface crystal designed for power intensity ratio control via selective stimulation.

In the first instance, the pump waist location along the composite crystal length was horizontally translated within such a distance as to effectively vary the physical volume that is optically stimulated by the pump thus directly altering the pump photon concentration incident on the crystal ends in favor of either the Nd:YVO_4 or Nd:$GdVO_4$ [16]. In the more recent alternative implementation, the composite crystal used had an angled vertical interface between the two bonded vanadate components

and the incident pump beam longitudinally imaged onto the crystal was again translated, but this time it was done laterally in order to vary the horizontal location of the pump waist along the wedged interface of the designed crystal in order to successfully control the intensity ratios of laser wavelength pair output as produced by each vanadate component [17]. Unfortunately in laser operation, mechanical translation of laser components inevitably introduces some measure of misalignment of the laser with direct degrading effect on its output power and stability.

In this study, a similar diffusion-bonded composite crystal of Nd:YVO_4/Nd:$GdVO_4$ was used. However, an entirely different approach was followed. The crystal was pumped at a longer wavelength specifically around 912/914 nm instead of the traditional ~808 nm in order to reduce quantum defect (QD) and consequently improve the slope efficiency. According to the material presented in Chapter 2, one of the key advantages of the longer pumping wavelength is the reduction of the energy difference between the pump and laser photons and consequently an appreciable decrease in the crystal lensing normally caused by thermal gradients within the crystal. Although the actual heat-induced lensing was not specifically measured, its reduction was indirectly verified by the recorded increase in output power and efficiency figures [9-12] as discussed in Chapter 3.

As an added innovation, the tuning of the spectral power ratio by means of the variation of the pump wavelength was experimentally demonstrated. This power ratio tuning was possible since the absorption of the GVO and YVO does not coincide (~912 nm vs. 914 nm) – as was determined from the data obtained from previous works [9-12]. The tuning was implemented by the temperature adjustment of the peak pumping wavelength of the laser diode pump. This conveniently moderated the respective gain of the either spectral output of the DW laser relative to the other. The variable excitation wavelength thus offered a simple "touchless" solution for the tuning of the power intensity ratios for this CW DW laser. The adopted long-wavelength pumping initiative follows from new

opportunities presented in recent works on in-band pumping of the Nd:$GdVO_4$ and Nd:YVO_4 crystals [18-20] as well as on some other crystals [21, 22].

Since the intention was to pump the laser at a longer wavelength specifically around 912/914 nm in order to reduce the difference in energy between the pump and laser photons and hence reduce heating within the crystal, the more desirable and significantly larger absorption coefficient at 808 nm was traded off for this purpose. In other words, it can be seen from the respective absorption profiles of the constituent components (Nd:YVO_4 and Nd:$GdVO_4$) of the composite crystal (shown in figures 2.5 and 2.6 in Chapter 2), that the absorption is grossly reduced at the longer wavelengths around 912/914 nm when compared to the absorption profile around the traditional pumping wavelength of 808 nm.

In a bid to compensate for the significantly reduced absorption, the crystal specification used was ordered to be made with relatively high concentration of dopants (typical doping level ranges from 0.2 till 1.1 at.%). Thus the Neodymium ions doping was made to concentration levels of 2 at.%. on either side of the composite crystal.

1.3 Objectives

This research was primarily focused on presenting a controllable CW DW laser based on a diffusion-bonded composite Nd:YVO_4/Nd:$GdVO_4$ crystal in which a simpler spectral intensity tuning technique was implemented. This technique involved the discrete variation of the laser diode temperature using a digital temperature controller, in order to provide a corresponding change in the pumping wavelength. The dual-wavelength laser operation was successfully demonstrated experimentally as an alternative turnkey means of controlling the power intensity ratios of the composite crystal of Nd:YVO_4/Nd:$GdVO_4$. The output from tuning the power intensity ratios for the spectral pair at various pumping wavelength (temperatures) was subsequently measured and

analyzed. It is noteworthy that this is the first time this initiative has been applied toward controlling power intensity ratios for dual-wavelength laser operation.

In addition, to scale the output power towards a higher potential, low QD pumping was used to pump the composite crystal in-band over the 910 - 914 nm range [10, 12, 13]. This pumping range was precisely targeted to achieve simultaneous excitation of either vanadate end of the crystal while also ensuring the delivery of a more power efficient DW laser performance facilitated by a reduction of the QD-induced heating within the composite crystal. This heat reduction achieved was evidenced by a relatively higher slope efficiency than was obtained in other works where pumping was performed at 808 nm using a similar crystal [3, 12, 15 - 17].

Overall, the stated study objectives were broken down into precise goals as outlined below namely:

- Validate that a high average output power can be obtained by pumping the Nd:$GdVO_4$/ Nd:YVO_4 crystal at 912/914 nm instead of the conventional 808 nm;
- Confirm that a high slope efficiency can be obtained corresponding to the high output power that results from the lower QD-induced heating of the crystal;
- Demonstrate the controllability of the dual-wavelength power intensity ratios using a temperature-dictated change in pumping wavelength that varies toward either 910 nm or 914 nm for the requisite stimulation of the Nd:$GdVO_4$ and Nd:YVO_4 ends of the composite crystal specifically around the 912 nm and 914 nm respectively.

1.4 Contributions

Based on the mentioned objectives, the contributions from this work include:

- Presentation of an operational in-band pumped CW dual-wavelength laser based on a Nd:YVO_4/Nd:$GdVO_4$ composite crystal with pumping wavelength around 910 - 914 nm;

- Demonstration of a novelty turnkey approach at controlling the intensity ratios of the individual spectral components of the dual-wavelength radiation using the temperature-controlled adjustment of the pumping wavelength;
- Exploitation of low QD pumping to obtain relatively higher average output power in dual-wavelength operation with a corresponding high quality laser beam output. This is attributable to the reduction in heating and the resulting reduced thermal gradients and lensing effects in the crystal.

As a note, the results of this thesis were presented (as poster presentation) at the Photonics North conference held in Quebec City, May 21-13, 2019 and are being prepared for a journal publication.

1.5 Thesis outline

The work undertaken in this research is detailed in the 4 chapters of this thesis. It would be presented according to the chapter-content sequence outlined below:

Following this introduction, the second Chapter is presented providing a quick theoretical overview. This covers fundamental understanding of dual-wavelength lasers, the low-quantum defect pumping technique around 910 - 914 nm; also, prior research in this area. In addition, a basic review of the composite crystal properties as an integral of the individual properties of Nd:YVO_4 and Nd:$GdVO_4$. Then, it concludes with an in-depth but brief review of the work on dual-wavelength operation as was done in previous studies.

In the third Chapter of this thesis, the details of the experiment and the setup used are provided. Other information included in this chapter are a description of relevant details of the laser diode pump, the design of the cavity, the pumping of the crystal and the temperature-adjustment of the pumping wavelength and then ending with a presentation and discussion of the results obtained.

Lastly in Chapter 4, a summary is documented on the research outcomes and it concludes with opportunities that may be explored in future research.

Chapter 2 - Theoretical Overview

2.1 Dual-wavelength lasers

DW lasers generally refer to the category of lasers that produce simultaneous spectral output at two different wavelengths [4 - 6]; this is the primary distinguishing factor between the DW lasers and the conventional laser which produces a single wavelength radiation. Different implementations of DW lasers have been designed with various setups based on single or dual-crystal arrangements using either one or multiple active materials or dopants [4]. Fig. 2.1 shows a dual wavelength output with two arbitrary emission lines.

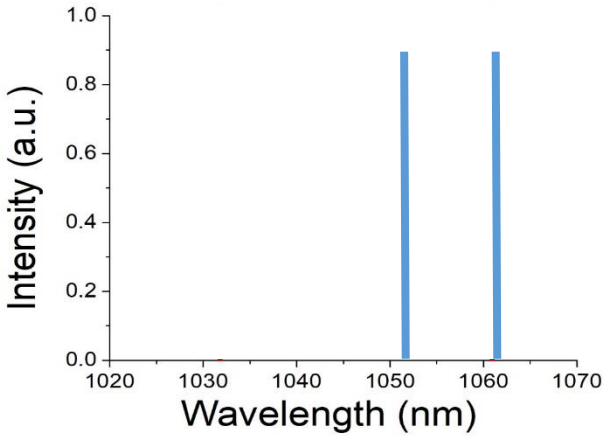

Figure 2.1 A pair of DW spectral lines

Some of the popular methods for achieving DW laser radiation include using a: coupled cavity [5], Birefringent filter [7], Fabry-Perot filter or specially bonded crystal [3]. The last method was experimentally used to demonstrate the efficient and controllable DW operation presented in this work. DW laser action from these implementations produce radiations and the wavelengths of the oscillating pair maybe determined by factors such as the gain medium characteristics [2, 7]. The DW separation as well as the stability and the tunability of the spectral power intensity ratio (between the

two lines) are important factors with regard to the utility of the DW lasers in applications for which they may be deployed [5, 6].

Laser host materials such as Yttrium and Gadolinium vanadates (YVO_4 and $GdVO_4$) are typically doped with rare-earth metals like Neodymium (Nd). The Nd dopant ions displace those of the host within its crystalline structure giving rise to the doped forms - Nd:YVO_4 or Nd:$GdVO_4$. The dopants in-situ effectively provide multiple active ion-bearing energy levels - a pre-requisite for multi-wavelength laser action in the doped crystals [1]. Simultaneous and independent dual or multi-wavelength oscillations can then be achieved from the field-determined stark-splitting within the crystal which yields multiple laser-feasible transition levels [1, 5].

By combining the emitted wavelength pair using special techniques such as the difference frequency generation (DFG) using a non-linear crystal [5], the optical beating of the dual laser frequencies can be used to generate stable and reliable terahertz (THz) frequency radiation. THz radiation is defined in the frequency range of 0.1 - 10 THz and is equivalent to 3 mm - 30 μm of wavelength [5]. It is the basis for a range of imaging systems used in applications that provide solutions to a variety of biomedical and security-related challenges.

THz radiation is mainly beneficial because of two key advantages. The primary reason is that it is able to go through most materials traditionally considered to be opaque (though this excludes metals). Secondly, it is able to provide high resolution and in-depth selectivity information of materials via its interaction with the materials through different mechanisms including but not limited to phonon, bond deformation and vibrations.

Thus, such information about material internal structure, thickness as well as physical or chemical composition may be obtained as changes in the pattern of the THz intensity and phase which is in

turn produced from the combination of the THz signal absorption and refractive index changes. Furthermore, THz signal is non-ionizing and so work great for biomedical applications since they are non-injurious.

2.2 Low Quantum Defect (QD) Pumping

Low QD pumping is an efficiency and performance improvement pumping technique. It basically involves pumping at a relatively longer pumping wavelength otherwise pumping directly into the upper laser band hence in-band pumping (as shown in figure 2.2), at a wavelength different than that known wavelength at optimum broadband absorption. This is done in order to simultaneously achieve excitation of the laser crystal and reap the benefit of a reduced QD as implied by the name.

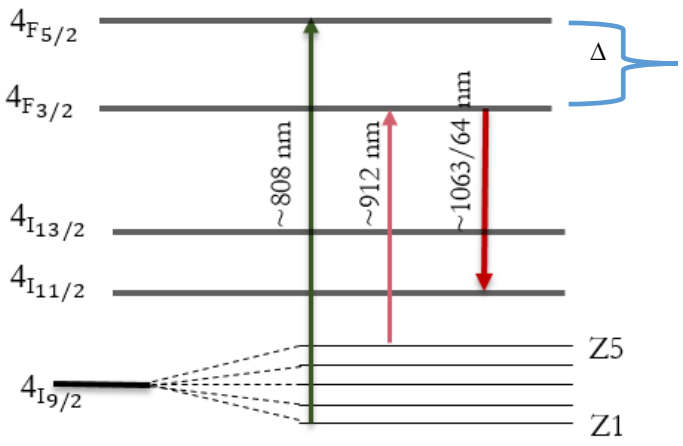

Figure 2.2 Low QD initiative by in-band pumping (into the upper laser band). Δ graphically illustrates the transition that leads to heat generation - now eliminated by pumping directly into the laser band using this technique

Traditionally, Nd:YVO_4 and Nd:$GdVO_4$ are pumped at wavelength of circa 808 nm which coincides with their peak broadband absorption [9, 15]. However, using low QD pumping, they may be pumped at some other longer absorption-feasible wavelengths such as between 910 and 914 nm [9 - 13] - as was used for the Nd:YVO_4/Nd:$GdVO_4$ crystal in this study.

Low QD pumping is inherently possible using 912/914 nm pump wavelength in either crystal based on the opportunities presented around that band in the absorption profile of both the Nd:YVO_4 and the Nd:$GdVO_4$ crystals. Furthermore, it is practically facilitated by the availability of laser diodes with emission spectrum around that exact desired pumping band [8] and so it was explored toward scaling the power output of the DW laser in this research.

It may be recalled from discussion on laser basics in the previous chapter that for steady state gain in solid-state lasers, population inversion in the crystal or gain medium is achieved and sustained by the use of some mechanism of excitation. Optical sources including arc and flash lamps or laser diodes are thus used to pump the laser crystal. However, lasers are subjected to significant heating originating from the very same pumping process [1]. On account of this heating tendency and the associated thermal complications which adversely affect the laser performance [6], lasers mostly require adequate design considerations to provide for effective thermal management [1, 4, 9].

The underlying cause of the identified heating issue in laser crystals was identified as being mainly from the notorious deposition of waste heat in the crystal host lattice which occurs progressively with pumping and laser action. That waste heat can be traced to the thermalization of the quantum defect (QD) which is the energy difference between the photons of the pump and those of the laser [1].

The two-part thermalization is contributed partly by the heat generated between the pump and the upper laser levels and additionally, the other portion emanates from between the terminal level of the laser and the ground state as in figure 2.3. The cumulative outcome from these is the detrimental heat generation named accordingly as QD heating [9, 10].

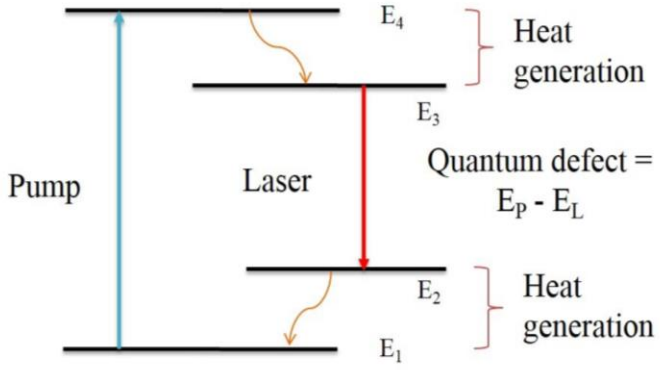

Figure 2.3 Quantum defect illustration for a 4-level laser. E_P and E_L depict the energy of the pump and laser respectively. E_1: Ground state, E_2: Lower laser level, E_3: Upper laser or metastable level, E_4: Pump or highly excited band. [© R. C. Talukder 2016] [21]

Heating due to QD, together with contributions from other non-radiative intra-crystal processes, leads to the development of a heat gradient across the crystal with deleterious consequences for the laser [15]. Among other limiting effects, QD heating rapidly culminates into the already-mentioned thermal lensing effect with its consequent reduction of lasing efficiency owing to the mismatch of pumping and lasing modes ultimately reducing slope and optical efficiency as well as hindering the achievement of high output power with increasing severity of the associated thermal effects [6, 10, 11].

A parameter η_F, fractional thermal loading, can be used to approximate the amount of crystal heating produced relative to the wavelengths of the laser and incident pump radiation [1].

Fractional thermal loading is evaluated as:

$$\eta_F = 1 - \frac{\lambda_P}{\lambda_L} \tag{2.1}$$

where, λ_P = pumping wavelength, λ_L = laser wavelength.

From equation (2.1), it can be deduced that the QD heating produced in the laser crystal will be progressively reduced as the difference between the wavelength of the pump and that of the laser (otherwise the quantum defect) is lowered. Thus, fractional thermal loading should tend toward zero as the pumping wavelength equals the laser wavelength.

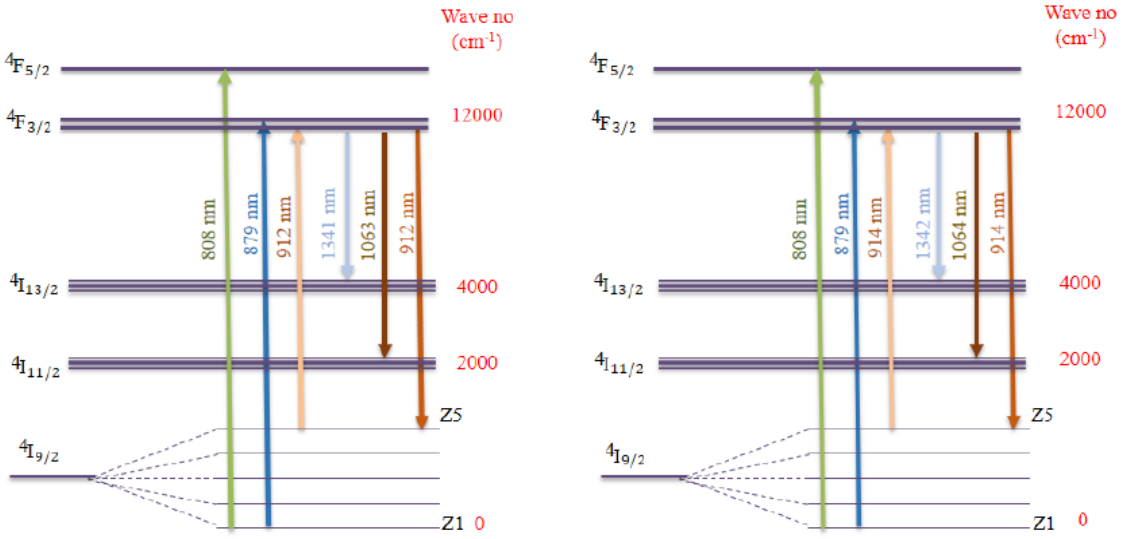

Figure 2.4 Schematic of pump and laser energy transitions with corresponding wavelengths for Nd:$GdVO_4$ (left) and Nd:YVO_4 (right) [© M. Nadimi 2018]

From the foregoing, low QD pumping provides numerous benefits such as increased efficiency and it also ensures a preservation of the high beam quality from vanadates [13]. The efficiency improvement arises via a direct reduction in the amount of waste heat deposited as is achieved with the lowered QD. Low QD pumping also favors generation of higher output power in the laser by exploiting the increased efficiency and leveraging the better pump power spread in the crystal since there is less pump absorption at the longer wavelength and the significantly reduced heat contribution from each emitted laser photon [4, 15]. From the diagrams in figures 2.2 and 2.4, it is clearly evident that a low QD can be achieved by pumping between the bands that provide the least energy difference

which is offered by the multiple stark-split energy levels [1, 5]. In other words, by pumping in-band directly into the upper laser level from the highest level of the ground state brings about less heating, distortions and losses.

Low QD pumping has been practically demonstrated with different crystals at varying wavelengths. For instance, low QD pumping for Nd:YVO_4 at 880, 914 nm [1, 11, 13, 15] and also at both 912 nm and 913 nm for Nd:$GdVO_4$ were noted from prior studies [9, 11]. In an original study using low QD pumping for Nd:$GdVO_4$ by J. L. Ma et al [9], a high slope efficiency of about 81.2% was achieved by pumping at 913 nm with power output up to 3.32 W. Also, 19.8 W output was obtained with a corresponding slope efficiency of 62.5% with a version further scaled by M. Nadimi et al. [10]. In theory, by using low QD pumping at 913 nm, it is possible and it has been shown to improve the quantum defect efficiency to 85.9% from about 83% (pumping at 880 nm); this is significant compared to the 75.9% imposed by the traditional pumping at 808 nm [11]. It has also been experimentally demonstrated that the lower heat deposition in case of 913 nm pumping resulted in thermal lensing reduction by about half the amount relative to when it is pumped at the traditional 808 nm [10, 11].

Low QD pumping offers a tested and operationally convenient means of enhancing thermal management via more efficient energy transitions. Since it provides heat management in part, it can serve to compliment other physical or spatial initiatives such as the modified crystal geometry, cavity design and heat sinking arrangements in order to optimally alleviate the performance-limiting problems due to crystal heating [1, 9 - 11].

2.3 Highlight of the Crystal Used

In this work, a single crystal of diffusion-bonded Nd:YVO_4 and Nd:$GdVO_4$ was used as the gain medium. The idea of a CW dual-wavelength laser based on a bonded composite crystal of Nd:YVO_4/Nd:$GdVO_4$ conveniently exploits the similarities in the lasing requirements, crystal properties and spectral output of both vanadates. This includes the ability to optically excite either component of the crystal within the same range of pumping wavelengths using a single pump source. Thus, this arrangement harnesses their known features and benefits towards the achievement of the intended controllable DW laser.

The constituents of the bonded crystal - Yttrium Orthovanadate (Nd:YVO_4) and Gadolinium Vanadate (Nd:$GdVO_4$) are two popular Nd^{3+} doped laser gain media of the crystalline variant normally used independently as laser crystals. Both vanadates are well established crystals and have been available for over two decades; they have been common choice in the design of solid-state lasers within output power limits of up to 20 W, lasing around 1.06 μm and with high beam quality [10].

As mentioned earlier, both the Nd:YVO_4 and Nd:$GdVO_4$ possess similar crystal structure and lattice parameters with a range of interesting spectral properties and they are particularly favorable for laser action with diode-pumping. Among some of the attractive benefits for the Nd:YVO_4 are its low lasing threshold, high pump light absorption coefficient and a broadband absorption band that is known to be at a maximum around 809 nm [1, 10, 13, 15]. Additionally, it has a remarkably large stimulated emission cross-section which is significantly larger than that of Nd:YAG - another popular laser crystal that lases at 1064 nm [1, 14]. Among other benefits, Nd:$GdVO_4$ offers superior heat handling as well as both absorption and emission cross-sections that are similar to that of the popular Nd:YAG crystal [1]. The plots in figures 2.5 and 2.6 show the polarization-specific absorption spectra for both vanadates used in this work.

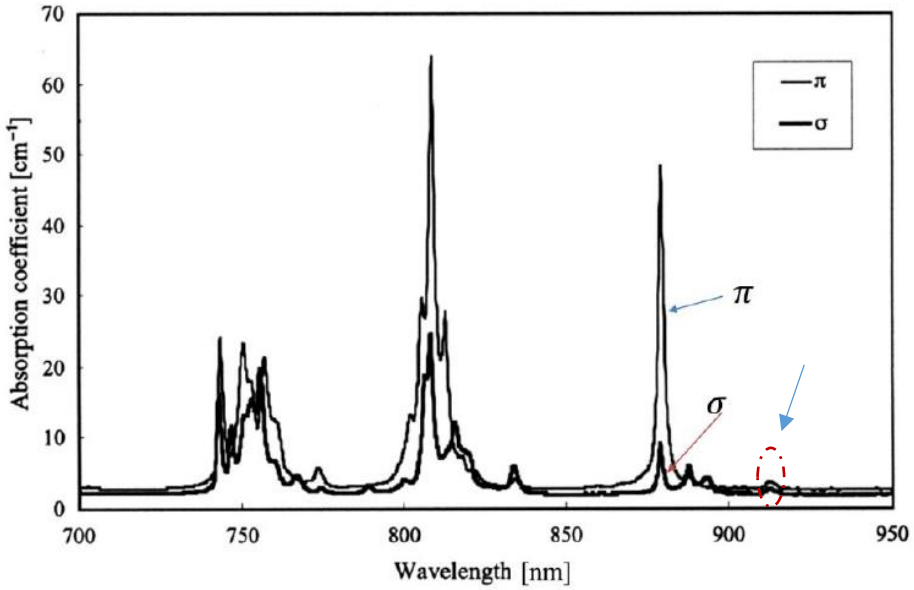

Figure 2.5 Absorption spectra for Nd: $GdVO_4$ [21]. The blue arrows (inset) highlight absorption 'bump' in the spectra around 912 nm. This was explored for the long wavelength pumping

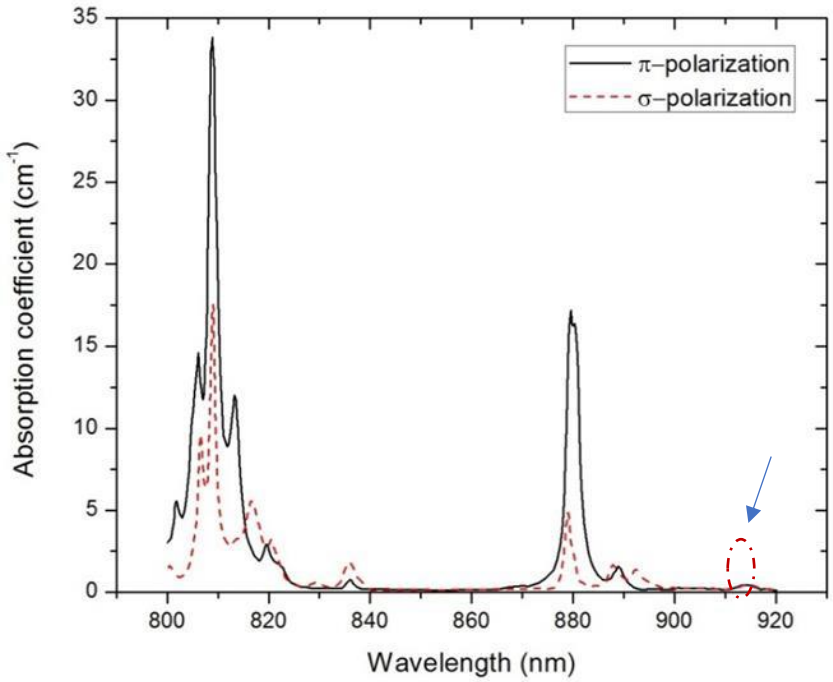

Figure 2.6 Absorption spectra for Nd:YVO_4 [20]. Blue arrows (inset) highlight absorption 'bump' in the spectra around 914 nm. This was explored for the long wavelength pumping

2.3.1 Nd:YVO_4

In terms of crystal properties, Nd:YVO_4 possesses lattice parameters **a** = **b** = 0.7118 nm and **c** = 0.6293 nm [15]. Nd:YVO_4 is uniaxial crystal with equal **a** and **b** axes but with a **c** that is different. It possesses a natural birefringence in addition to the laser-favorable combination of other spectral, physical, thermal and mechanical properties when compared to other similarly doped materials [9]. Nd:YVO_4 has a large stimulated emission cross-section and a significantly high gain [1, 3, 15]. Furthermore, it has a characteristically high pump absorption coefficient in addition to a broad pump wavelength acceptance.

Based on these characteristics, its crystal length requirement tends to be on the shorter side – typically around a few millimeters; this could however become a cause for concern with higher doping concentration due to the higher probability of increased heating within the small pump volume. It is traditionally pumped at 808/809 nm since its broadband absorption is maximum at around same value, specifically at about 808.6 nm [15]. It is known to absorb pump radiation based on its polarization, with predominant inclination toward incident radiation of same polarization as its laser. It equally yields laser radiation that is linearly polarized [14].

Due to its large stimulated emission cross-section, even with a short upper state lifetime of about 91 μs, Nd:YVO_4 still has a low laser threshold for CW laser operation as determined by the inverse of the product σ and τ, of the stimulated emission cross-section σ and upper state lifetime τ [1, 5]. Nd:YVO_4 has peak emission lines at 914 nm, 1342 nm and 1064 nm in order of increasing emission intensities [5, 13, 14].

The energy levels within the Nd:YVO_4 crystal with pumping and lasing transitions for Nd:YVO_4 are shown in the figure 2.4. Following the hint from results of previous studies for the maximum

absorption for Nd:YVO_4 using low QD pumping in the 910 nm - 915 nm band [13, 15], the DW laser for this study was pumped at a maximum of 914 nm and this was precisely targeted at stimulating the Nd:YVO_4 component for optimum results . Thus exploring pumping transition proceeding through $4I_{9/2}$ to $4F_{3/2}$ and the ensuing laser radiation via transitions proceeding from $4F_{3/2}$ to $4I_{11/2}$. As can be seen from figure 2.6, absorption of light at 914 nm is much smaller than at 808/809 nm. This trade-off can be offset by using a longer crystal or higher doping level.

Apart from its relatively short upper state lifetime, a notable restricting property of the Nd:YVO_4 is its thermal conductivity. This parameter with value of around 5.1 W/m/K [5], in conjunction with other factors, determines the ease with which a crystal loses generated heat. It limits the ability to obtain high power output in their laser operation [9, 10, 15] and occurs because of their greater susceptibility to the thermal effects that cause optical distortions and losses with a possibility of crystal fracture if heating progresses uncontrolled [2].

2.3.2 Nd:$GdVO_4$

Gadolinium vanadate (Nd:$GdVO_4$) is a relatively more recent crystal compared to the Nd:YVO_4 and the Nd:YAG. Compared to these two crystals, it has a much higher pump light absorption. Nd:$GdVO_4$ has about half the size of the emission cross-section of Nd:YVO_4 but boasts of a similar lattice parameters and combination of advantages as Nd:YVO_4 [24] as highlighted in the previous section. Furthermore, it has a much higher capacity for handling heat [25], with a thermal conductivity of about 11.7 (W/m/K) which is over twice that of Nd:YVO_4 [1]. This gives it an edge over the Nd:YVO_4 which has less favorable thermal handling ability with thermal conductivity figure of 5.1 (W/m/K) [24]. Long wavelength absorption occurs around 912 nm with similar consequences as in the case of Nd:YVO_4 as can be seen from figure 2.5.

Thus, with both vanadates bonded in the composite crystal, the superior thermal conductivity of the Nd:$GdVO_4$ was exploited by making it the facing side for the incident pump radiation. This arrangement effectively compliments the Nd:YVO_4 with its twice better thermal conductivity. More properties of the neodymium-doped yttrium vanadate and gadolinium vanadate are detailed in table 2.1.

Table 2.1 shows some properties for both vanadates for the 1063/1064 nm laser transition (considered for 0.3 at.% and 0.5 at. % for Nd:YVO_4 and Nd:$GdVO_4$ respectively) [5]

Properties	**Nd:YVO_4**	**Nd:$GdVO_4$**
Laser wavelength $\boldsymbol{\lambda_L}$ (nm)	1064	~1063
*Emission cross section $\boldsymbol{\sigma_{em}}$ (10^{-19} cm^2)	15.6	7.8
*Gain bandwidth $\Delta\boldsymbol{\lambda}$ (nm)	~1	~ 1
*Fluorescence lifetime τ (μs) (1% doping)	~90	~90
Thermal conductivity $\mathbf{k_C}$ ($Wm^{-1}K^{-1}$)	~5.1	11.7

** May vary with change in doping concentration*

2.4 Previous records of DW Nd:$GdVO_4$ /Nd:YVO_4 lasers

In 2010, A.J. Singh et. al. [5], reported on a DW laser study, acclaimed as the first using a hybrid arrangement of two separate Nd:$GdVO_4$ and Nd:YVO_4 crystals with length of 7 mm and 12 mm respectively [4, 5]. In this study, both crystals were placed side by side in close proximity and each was doped with due consideration of the previously highlighted pumping-associated thermal problems and because of this, the shorter Nd:$GdVO_4$ crystal was doped with 0.5 at.% and with just 0.3 at.% doping for the Nd:YVO_4 to compensate for its lower thermal conductivity. The entire configuration was end-pumped in a single linear cavity. The crystals were pumped at the traditional 808 nm for the DW laser operation at 1.06 μm. However, two different laser diode pumps were utilized in order to

independently control their emission intensities and corresponding power intensity ratios by overcoming constraints around gain competition between both crystals [5].

Further DW laser studies using a composite crystal of both vanadates were subsequently undertaken starting with the work presented in 2015 by Y. J. Huang et. al. [4]. The authors designed a DW laser using a single diffusion-bonded crystal of Nd:$GdVO_4$ and Nd:YVO_4 with doping concentration of 0.5 at.% and 0.2 at.% respectively; the bonded crystal utilized had a length of 10 mm corresponding to 3 mm for Nd:$GdVO_4$ and 7 mm for the Nd:YVO_4. They achieved equal absorption and successfully demonstrated simultaneous laser action with dual emission wavelengths of 1063.18 nm and 1064.37 nm. This DW laser using a 95% reflectivity output coupler produced an average power output of 1.1 W from 5.1 W of incident pump power thus yielding a slope efficiency of about 24% [9].

Following the success of that original work, attempts at improving and controlling the power intensity ratio of the DW laser saw two other particularly interesting tuning initiatives [16, 17]. The techniques, previously described in brief in the first chapter of this report, proved effective for controlling the DW spectral intensity ratio albeit requiring some measure of mechanical adjustment of either the laser crystal or pump source. The initial technique specifically involved moderation of the relative gain in the diffusion-bonded crystal of Nd:$GdVO_4$/Nd:YVO_4 using a linear translation stage to vary the pump beam waist within the crystal [26] while with the latter technique, a specially designed crystal with a wedge geometry interface between both components of the composite crystal was used. This provided another means of selectively adjusting the relative gain between the two components of the crystal. In either case, not more than 2.5 W of average output power was obtained with slope efficiency of just about 27% [4, 18].

In a different study in 2017, F. L. Chang et. al. [16] using a similarly wedge-shaped composite crystal of Nd:$GdVO_4$/Nd:YVO_4 with same doping and length specifications as used by Y. J. Huang [4]

demonstrated a dual-central-wavelength laser and experimentally tuned the DW emission. The tuning was achieved with gain moderation based on the geometry of the crystal. They, thus, revalidated control of the power intensity for the DW lines based on the vertical location of the beam in the specially shaped crystal. The report also indicated that an output power 2.7 W was obtained from 13 W of pump power [12].

Table 2.2 compares the performance from previous DW lasers using crystals that are composites of Nd:$GdVO_4$/Nd:YVO_4. From the figures presented, it is evident that previous designs have been restricted in efficiency and thus output power.

Table 2.2 Performance summary for some previous DW lasers using composite crystals

Authors	**Year**	**Maximum Incident Power (W)**	**Average Output Power (W)**	**Optical-to-Optical efficiency (%)**	**Slope efficiency (%)**	**DW Power Intensity Ratio (P_{1063}/P_{1064}) Tuning**
Y.J. Huang et. al. [3]	2015 #1	5.1	1.1	21.5%	~24.2%	Not attempted
Y.J. Huang et. al. [26]	2015 #2	14	2.9	~20.7%	22.3%	Tuned by linear variation of the pump waist within the crystal
Y.J. Huang [16]	2016	21.6	6.4	29.6%	--	Tuned by linear variation of the pump waist within the crystal
F.L. Chang et. al. [14]	2017	13	2.7	20.8%	22%	Tuned by linear variation of the pump waist within wedge-interface crystal
Hsin-Chih Liang et al. [18]	2018	11	2.5	22.7%	25%	Achieved by vertical variation of the pump waist within crystal
Current work	2018	11.55	4.48	38.8	43.8%	Achieved by temperature-controlled variation of pump wavelength

Chapter 3 - Experimental setup and Results

3.1 Crystal specification and setup

It was previously mentioned that the gain medium used in this study was a custom-made crystal of Nd:YVO_4 and Nd:$GdVO_4$, bonded by diffusion to form a composite single element. The length of the crystal used was 10 mm, made up of equal-part (5-mm-long) a-cut of both Nd:YVO_4 and Nd:$GdVO_4$. Each side of the vanadate was highly doped with concentrations of 2 at.% to compensate for the reduced absorption for both vanadates at the longer pumping wavelength (912/914 nm). The bonded crystal had a cross sectional dimension of 3 mm x 3 mm and was pumped longitudinally along its length as depicted in the color-coded schematic in figure 3.1.

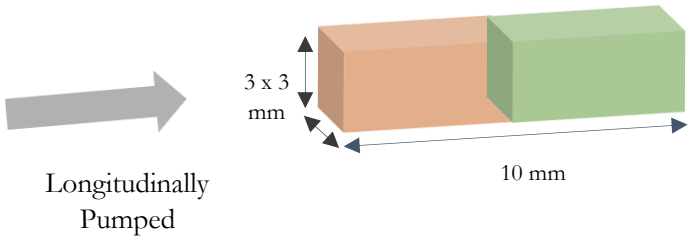

Figure 3.1 Color-coded schematic showing composite crystal geometry and direction of pumping

Considering that end-pumped systems are relatively more prone to non-uniform heat deposition compared to other pumping configurations like side pumping, a choice of medium and method for cooling the crystal directly had to be made from arrangements based on air, water or thermoelectric cooling. Water cooling was conveniently adopted for being the most popular choice, as well as being readily available and the ease of its incorporation with the laser set up in the lab.

The crystal was thus wrapped in indium foil and water-cooled to 18℃. The arrangement ensured that heat from the crystal was exchanged directly from its top and bottom surfaces via the foil interface between the crystal and the holder stand as shown in figure 3.2. The images below show the crystal

sandwiched between the two aluminum water-cooled blocks and the water chiller in figure 3.3 provided the supply of continuously circulating cooling water at the designated temperature.

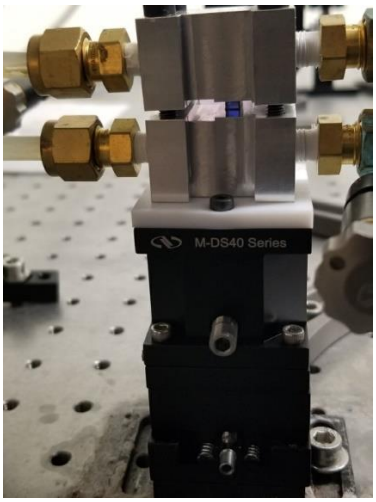

Figure 3.2 Crystal cooling arrangement. Indium foil-wrapped-crystal (tiny blue material) sandwiched in metal holder

Figure 3.3 Recirculating water chiller of the cooling system for laser. Digital displays show both the room temperature (to the left) and the temperature of the water in the cooling system (to the right) as at time of snapshot

3.2 Laser diode pump

The pump source used for this experiment was a laser diode that provided the required optical excitation. This source was coupled via lenses using a fiber possessing a 105 μm core diameter and a numerical aperture (NA) of 0.22. Using these focusing optics, the pump was imaged onto the mid-area of the crystal with a spot size radius of ~262.5 μm. The laser diode was temperature-controlled within the 910 - 915 nm band using a thermoelectric cooling arrangement. The diode was placed on a cold plate based on thermoelectric (Peltier) elements. The pump was precisely operated in the specified wavelength range to lower QD in the laser - as explained in the previous chapter. A picture of the diode pump setup is shown in figure 3.4.

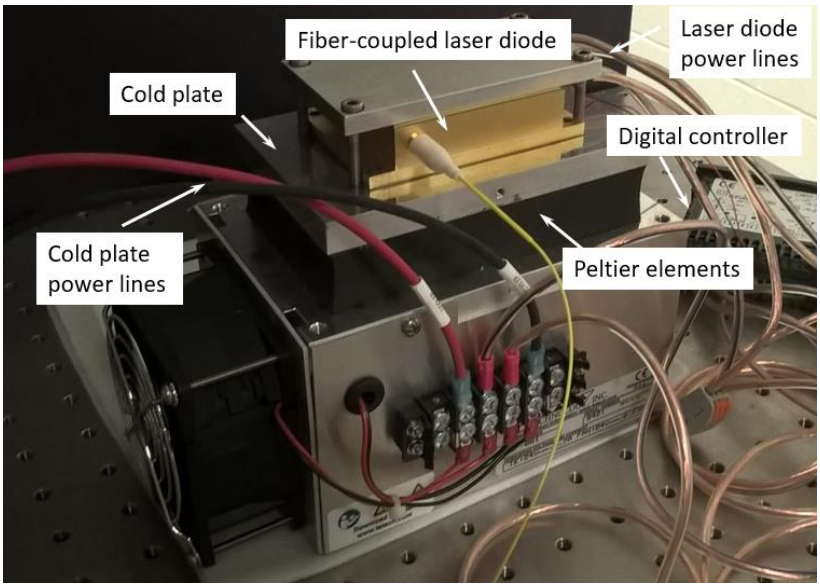

Figure 3.4 Laser diode cooling setup with temperature control

In addition to serving as the excitation source, the laser diode pump also served as a means of conveniently tuning the DW spectral lines of laser by moderating the gain between the two vanadate sides of the composite crystal. The technique in this case exploited an inherent ease of wide range wavelength tuning for laser diodes based on their sensitivity to heating. More specifically, the inverse

response of their energy bandgap to temperature changes which is seen in the corresponding shifted peak wavelength outputs. Notably, when the temperature of the diode is increased, the bandgap energy the diode is decreased producing a longer peak wavelength output. Conversely, when the diode temperature is reduced, its energy bandgap is increased, leading to a shorter peak wavelength output.

Based on the theory above, the temperature of the laser diode was adjusted by means of an in-built thermistor which was operated over the range between 27 - 39℃ using a digital controller. This was done in order to facilitate the temperature-dictated variation of the pumping wavelength. The spectral output from the laser diode pump over the stated temperature range was analyzed with a spectrum analyzer and it was in alignment with theory showing the shifting pump wavelength in response to the changing temperature as expected.

The output obtained is displayed in plot of diode wavelength versus operating temperature shown in figure 3.5. Each required adjustment of the laser diode operating temperature T_{LD} was achieved by simply entering the required temperature figure by means of a keypad into the digital controller for the pump. Increasing the temperature of the laser diode directly resulted in a corresponding increase in the pumping wavelength and vice versa when it was decreased. The wait time for each temperature transition and stability was observed to be a function of the temperature difference between the current operating temperature and the intended or final temperature. On the average, the wait time was no longer than two minutes for all selections in the operating range for the tuning between 27 and 39℃.

Using this technique, the tuning the power intensity ratio (P_{1063}/P_{1064}) of the DW lines for the laser was demonstrated by simply adjusting the peak pumping wavelength from 909.8 nm through 914.5 nm over the cited temperature range.

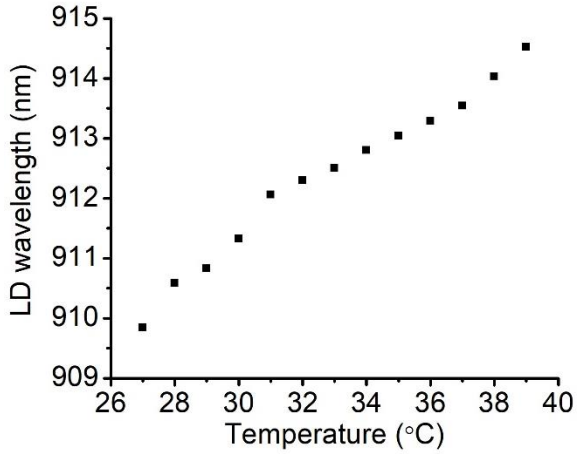

Figure 3.5 Plot of shifting peak wavelength for the laser diode due to temperature variation

3.3 Cavity modeling and design

A key consideration in the design and modeling of a laser cavity is to ensure that the laser beam and that of the pump are properly overlapped in the gain medium [1]. Achieving this objective, also known as mode-matching, is usually done by the precise spatial matching of the pump or excitation beam and that of the laser cavity beam sizes along with their divergences. This is simulated on a software package and then implemented in the lab.

Mode-matching, previously discussed in chapter 2, is an important laser requirement and it is necessary in order to obtain high optical-to-optical and slope efficiency in the steady-state operation of the laser as compared to operation in otherwise mismatched conditions when photons produced in the gain medium do not couple into the laser cavity mode. Hence for the design of the cavity, the choice of optical elements and their separation distances were made accordingly to satisfy that fundamental requirement.

The reZonator software was used to model the cavity, simulate its operation and optimize the performance [27]. Several other software programs and applications are available for the same purpose

including ASAP, LASCAD and GLAD to mention just a few. These programs rely on the ABCD matrix for the prediction of a Gaussian beam parameters (Appendix A contains more details on this).

A very common 3-mirror cavity configuration was modeled in the reZonator application as seen in figure 3.6. The cavity was comprised of the dichroic mirror (DM), curved mirror (M1) and output coupler (OC) mirror. The cavity contained laser crystal (LC) with induced thermal lens (F1) in the middle.

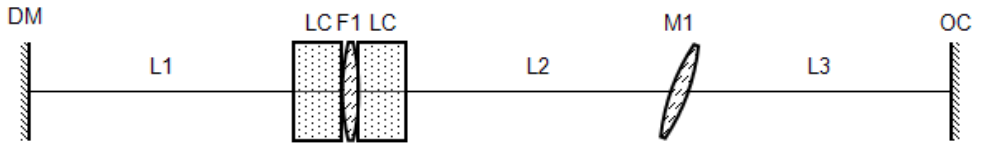

Figure 3.6 reZonator-generated schematic of the modeled DW laser cavity

These cavity elements were selected from the component categories within the application and were then put together sequentially. The configuration parameters like the free space separation between the optical elements were arbitrarily specified initially. Other user-defined parameters such as the refractive index for the crystal, the radius of curvature for the curved mirror (used), were specified in the software soon after. Then necessary adjustments were made repetitively per element and parameter while trying to fine tune the laser cavity mode size in the crystal to meet the desired (i.e. pump spot) size. For instance, the distances between them were checked to be reasonable, slightly decreasing or increasing (+/- 5mm) as required in order to accommodate physical constraints imposed by the actual dimensions of the mirrors and crystal holder.

Using the relay optics (the pair of collimating and focusing lenses shown in figure 3.8), the pump beam was (to be) focused onto the crystal around its mid area. The focal length of the collimating lens used

was 40 mm while that of the focusing lens was 200 mm. Together the pair imaged a pump beam size about five times the original beam size in the fiber onto the center of crystal. Hence, since the fiber core diameter used was 105 μm, the pump beam diameter was around 525 μm. The 1:5 imaging magnification for the pump spot size was designed specifically because of the divergence of the pump in order to maximize the overlap of the pump with the cavity mode along the crystal length.

So, in order to achieve that all-important primary objective of ensuring good mode-matching of the pump and laser beams as earlier mentioned, the modeled cavity with its optical elements and parameters were simulated to produce a laser beam that spatially matched that of the pump (~262.5 μm radius) within the crystal as in figure. 3.7.

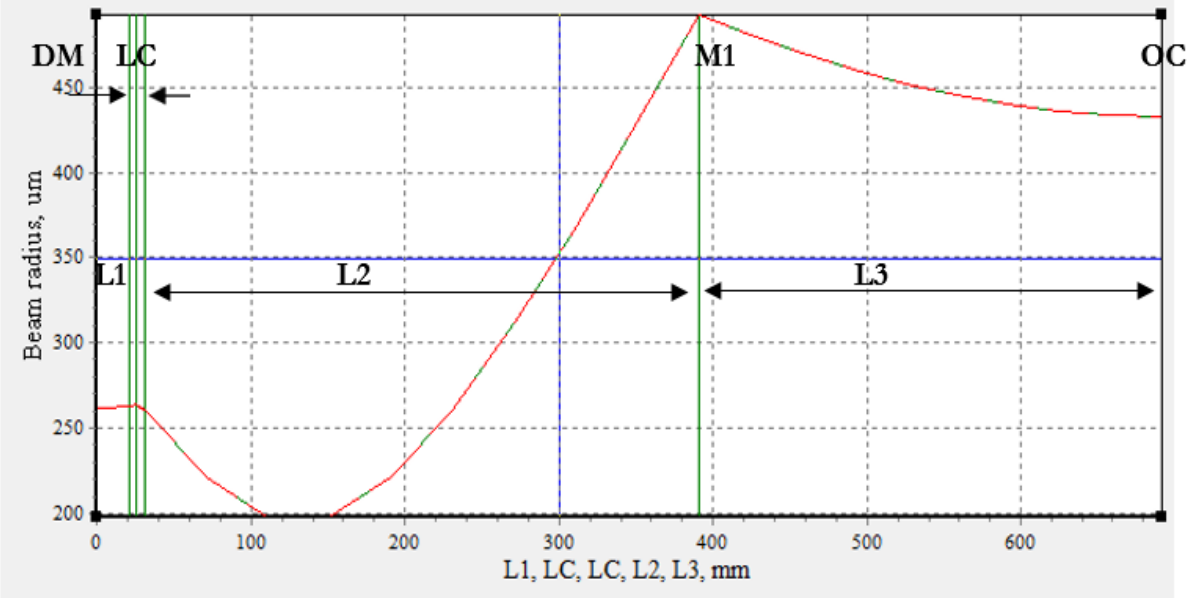

Figure 3.7 Screenshot of reZonator showing the changing beam radius of the laser propagating in the cavity

In this way, the free space separation requirements as well as the optical parameters necessary for the simulated mode-matched operation were determined and the same condition was set for replication in the actual laser in the lab.

The schematic of the cavity is shown in figure 3.8 while figure 3.9 shows the actual setup as implemented in the laser lab. The cavity had the following elements: **M1** - which is a concave mirror with 500 mm radius of curvature, the flat dichroic mirror (**DM**) with high reflectivity (HR) at 1063 nm and high transmission around the pumping wavelength of 912 nm. The choice of output coupler was made from a selection of up to four different output couplers with transmissivity ranging from 2.5 to 15%. The output coupler (**OC**) with 7.5% transmission was used since it provided optimum output power performance. In the schematic shown, **LC** depicts laser crystal whereas the separation distance between the elements are denoted as **L1**, **L2**, **L3** were 2.1, 36 and 30 cm respectively. Special considerations were also made for the commonly occurring solid-state lasing effects such as the thermally induced crystal lensing. Although normally varying in severity and uniformity within the crystal, it is usually modelled as a thin lens of certain focal length or dioptric power in the center of the crystal. This parameter was thus modeled as a thin lens (F1) positioned at the center of the crystal (LC) with a focal length of around 200 mm. The figure used for modeling it in this work is supported by data obtained from other research [10, 11].

Having satisfied the mode-matching requirement, implementing and tuning the laser was done systematically per component. First, the required optical components and elements for the cavity were physically identified and selected. Their separation was measured with a metric ruler and they were placed as required following the reference model in reZonator, but within +/- 1 mm accuracy. Then, finely varying component alignment and the laser beam spot size by means of manual translation of the components while monitoring the laser output power on the power meter ensured that the cavity stability limits were not reached. Component misalignment was noted and corrected as identified. Misalignments usually cause beam tilting with the consequent lateral displacement that leads to losses usually noticed in the form of output power reduction. In the extreme cases of reaching and overshooting the stability limits of the cavity, there was abrupt cessation of laser action with power

readings dropping to a minimum or zero. By means of a beam profiler setup with a dichroic mirror to filter out residual pump power after the output coupler, the transverse intensity map of the produced laser beam was monitored concurrently. Ultimately, the cavity was optimized to produce the highest output power in the fundamental Gaussian beam mode.

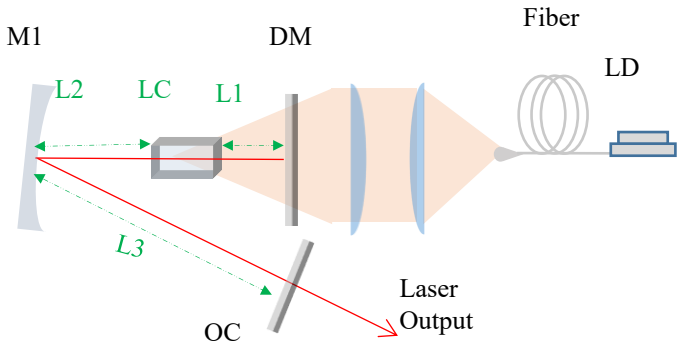

Figure 3.8 Schematic of the experimental laser setup

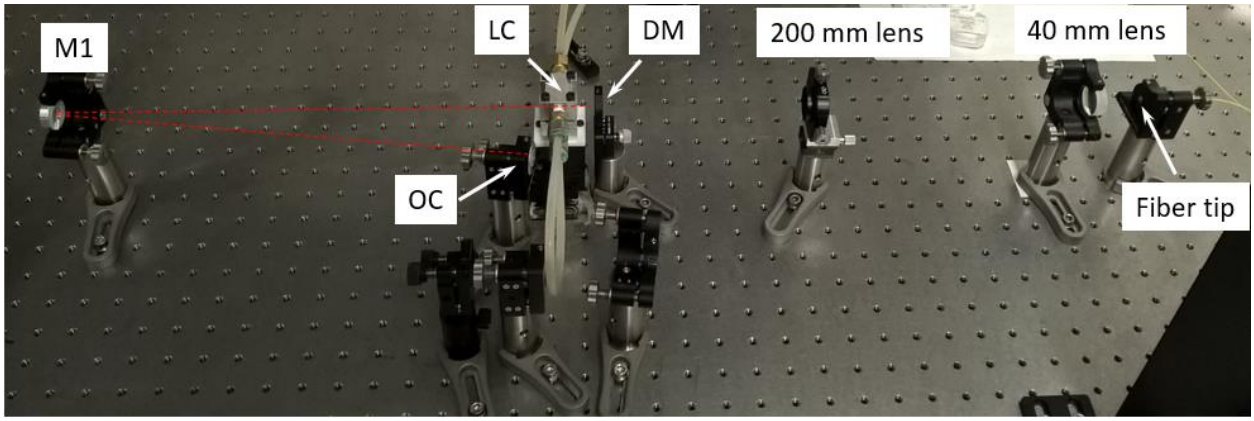

Figure 3.9 Photograph of the actual laser cavity setup. Red dashed line shows intracavity laser beam path

3.4 Results and discussion

Using the cavity and parameters as was obtained from the previous section, the total output power of the DW laser with spectral output at about 1063 & 1064 nm was measured against the absorbed pump power under the laser diode peak excitation wavelength (λ_{LD}) of ~ 912.5 nm. This is graphically depicted in figure 3.10.

The plot shows the output power as a function of the absorbed pump power. From observation and the experimental data recorded during the laser operation, there was no output until the threshold pump power was exceeded at which point the steady-state gain overcomes intra-cavity losses. Beyond that point and with increasing absorbed pump power, the laser output is obtained and sustained. The output power was seen to rise linearly with increasing pump absorption.

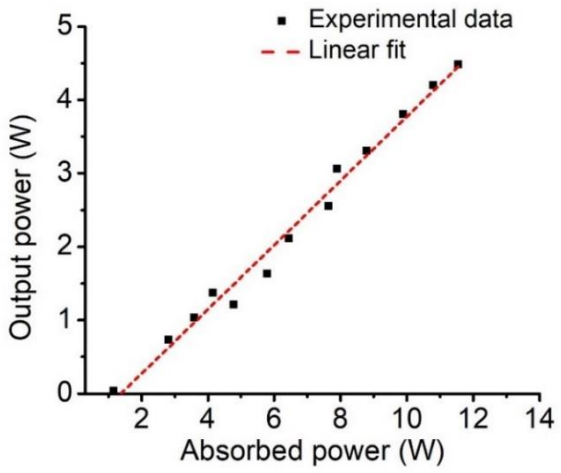

Figure 3.10 Dual-wavelength output power versus the absorbed pump power (Temp. 30 ºC)

This performance trend is sustained until the maximum output power was reached, noted to be 4.48 W. That maximum output power was obtained from 11.55 W of absorbed pump power. This result effectively corresponds to an optical-to-optical efficiency of 38.8% and a slope efficiency 43.8%.

Furthermore, the pump absorption efficiency for the laser was calculated to be around 60% given that the maximum incident pump power was approximately 19 W.

From the result obtained above, this work presents a marked improvement in performance compared to previous works. It is evident that the pumping technique method adopted by providing excitation with low QD pumping using 912/914 nm wavelength was the key distinguishing factor that provided a leeway towards attaining this significant leap in performance. Thus, as a result of that reduction in QD, the slope efficiency achieved here is remarkably higher and nearly doubles that obtained in the results in the other works. At the same time, a higher output power is achieved relative to those works for which a similar crystal was used. For more details, see table 2.2 in Chapter 2.

To further analyze the contribution as seen in the results here, it is worthwhile to recall that without the adoption of the in-band pumping method, the energy gap between the pump and laser photons places a constraint on the slope efficiency which is the gradient of the laser output power with respect to the pump power. The closer the pumping wavelength approaches that of the laser, the higher is the slope efficiency.

This can be observed from the relationship shown in equation 3.1 [1]. It expresses the dependence of output power on pump power as well as on the excitation and lasing wavelength among other contributions from the included cavity parameters.

$$P_{out}(T) \approx \frac{T}{T + Lc}\,\eta_a\left(\frac{\lambda_P}{\lambda_L}\right)(P_{Pinc} - P_{th}) \tag{3.1}$$

Where,

P_{out} = Output power, P_{Pinc} = Incident pump power, P_{th} = Threshold pump power,

T = Transmission of the output coupler,

Lc = Intra cavity losses,

η_a = Ratio of pump beam waist to that of the laser beam,

λ_P = Pump wavelength,

λ_L = Laser wavelength.

Based on the various options to scale output power and efficiency, increasing the pumping wavelength to 912/914 nm (instead of the traditional 808 nm) relative to a fixed lasing wavelength of 1063/1064 nm delivers significant benefits in terms of higher slope efficiency which depends on the ratio of the pump and laser wavelengths (see Eq. 3.1). Additionally, as has been demonstrated so far, the highlights of this approach proceed from the fundamental improvement in thermal management leading to more efficient lasing action and a substantial reduction in the thermally-induced lensing which was previously measured to be reduced even by as much as half that obtained using the traditional pumping [10, 11]. It is consolidated in the output power which is increased since thermal lensing is weaker and so there is less optical beam distortions or aberrations that cause mismatch between the pump and laser modes. Therefore, long wavelength pumping approach allowed us to achieve both higher slope efficiency as well as output power as suggested by Eq. 3.1.

The laser beam quality or propagation factor M^2 was measured using a beam profiler. This parameter provides a comparative figure for the quantitative evaluation of the extent of deviation of the laser beam relative to the diffraction limit for an ideal Gaussian beam. $M^2 = 1$ for an ideal Gaussian beam.

In this study, it was measured by focusing the laser beam onto a beam profiler using a focusing lens. This lens was placed at a fixed point from the output coupler (OC) beyond a pump 'filtering' lens.

The spot size of the beam was measured along the direction of propagation and it was found to be less than 1.05 in both the horizontal and vertical directions at full power operation. Relative to the ideal situation cited above, this laser produced an excellent beam quality and shape. Figure 3.11 shows the measured beam shape, beam radii and the beam quality factors along the x and y axes. The beam shape can also be seen in the image inset. Excellent beam quality points out to the fact that laser cavity design and subsequent optimization resulted in good mode matching between the pump and laser modes.

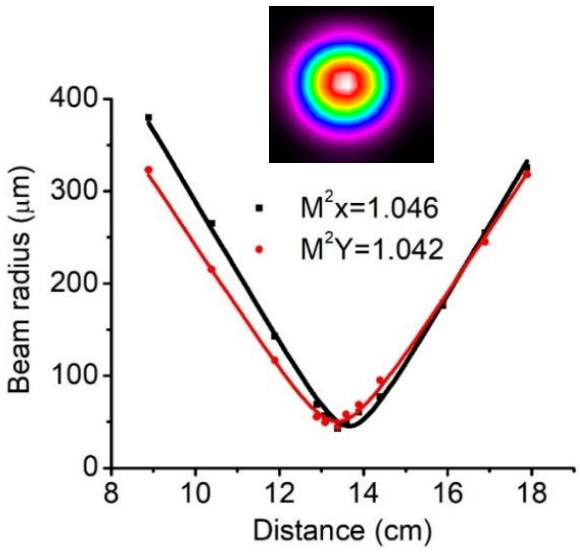

Figure 3.11 Laser beam quality measurement at full output power and the output beam shape (inset)

Recalling that increasing the temperature of the laser diode pump caused its output λ_{LD} to be shifted towards the longer wavelengths, operating the temperature of the laser diode from 27 °C to 39 °C caused λ_{LD} to be adjustable from 909.8 nm to 914.5 nm as shown in Fig. 3.12. The distinctive wavelength shift is shown at three specific temperatures for the laser diode namely: 29 °C, 36 °C and

39 °C. The corresponding emission spectra at those temperatures have peaks at 910.8 nm, 913.3 nm and 914.5 nm respectively. The full-width at half maximum (FWHM) was measured to be circa 3 nm.

Since the absorption peaks of the composite crystal coincide with those of its integral ($Nd:GdVO_4/Nd:YVO_4$) components - the first peak around that of the $Nd:GdVO_4$ at circa 912 nm and the other determined by the $Nd:YVO_4$ around 914 nm, the output power ratio of the laser was thus expected to be tunable while being pumped over this wavelength range. This tunability was experimentally demonstrated as depicted in spectral output shown figure 3.13.

Here, the measured spectra of the dual-wavelength laser at three different temperatures of 30 °C, 33 °C and 36 °C are presented. The DW laser peaks are clearly located around 1062.83 nm (~1063 nm) and 1063.95 nm (1064 nm). The origin of the small wavelength shift of the 1064 nm line as seen in figures 3.13(a) and (c) is not understood but readily supported by the available gain bandwidth of ~1 nm of this transition [1].

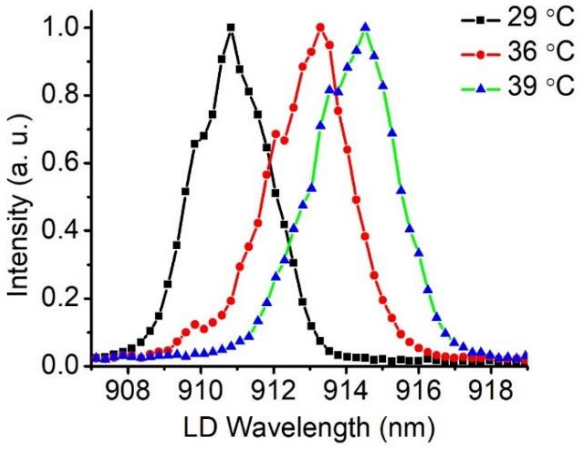

Figure 3.12 Laser diode spectra at 29 °C, 36 °C and 39 °C

The changing intensity between the DW laser lines followed the changing pumping wavelength validating the controllability of the output power ratio via the same means. The experimentally measured and normalized laser intensity at 1063 & 1064 nm as a function of the laser diode peak wavelength in the full range of 909.8-914.5 nm is shown in figure 3.13.

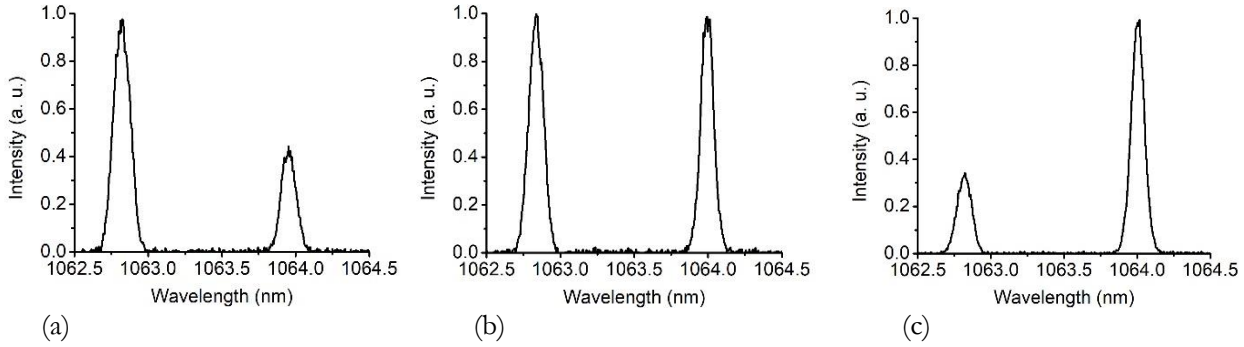

Figure 3.13 Dual-wavelength operation spectra at circa 1063 and 1064 nm. (a) - (c) Control of the power ratio between the two lasing wavelengths achieved by temperature-determined peak pumping wavelength of the laser diode. (a) λ_{LD} = 911.3 nm (T_{LD} = 30 ºC), (b) λ_{LD} = 912.5 nm (T_{LD} = 33 ºC) and (c) λ_{LD} = 913.3 nm (T_{LD} = 36 ºC). Where T_{LD} = is the operating temperature of the laser diode

From the output shown in the figure above, the changing relative emission intensities, either line of the DW laser changes as a result of pumping wavelength λ_{LD} varying in favor of the absorption for either the Nd:$GdVO_4$ or the Nd:YVO_4 component over the applied wavelength range. However, both intensities appeared to be in equilibrium (P_{1063}/P_{1064} = 1) around 912.5 nm pump wavelength. For λ_{LD} below 912.5 nm, the intensity of 1063 nm radiation is greater than of the 1064 nm. This is supported by relatively higher absorption of the Nd:$GdVO_4$ crystal below 912.5 nm. Conversely, above the 912.5 nm, the performance is reversed in favor of 1064 nm due to the higher absorption of Nd:YVO_4 compared to Nd:$GdVO_4$. This is shown in the plot in figure 3.14.

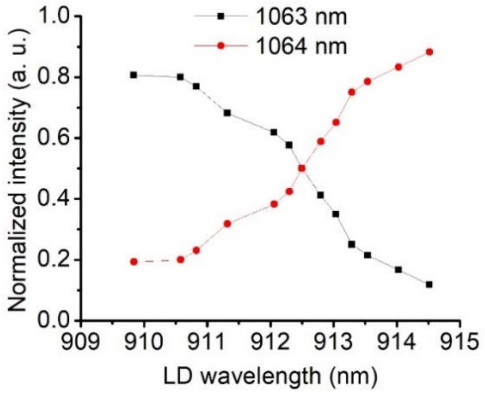

Figure 3.14 Normalized laser intensity at 1063 and 1064 nm as a function of the laser diode peak wavelength

Looking at figure 3.14 it should be noted that the total output power reached its maximum at 912.5 nm of pump wavelength. Moving away from this point in either direction resulted in gradual output power decrease. This can be explained by the fact that optimal excitation of both crystals took place at 912.5 nm and in other situations only one of the crystals was effectively excited and contributed to the lasing process. Comparing the obtained results with the those of other similar DW implementations as reviewed in table 2-2 of the final section in Chapter 2, this work among other advantages, provides a better DW laser in terms of its performance - with the remarkably higher output power and also the higher optical and slope efficiencies which can be attributed to the use of a low quantum defect pumping and the power intensity tuning approach.

Chapter 4 - Conclusion and future work

A controllable DW laser operation was experimentally demonstrated using a composite vanadate crystal. The laser was stimulated using low QD pumping technique in order to ensure waste heat reduction, increase in slope efficiency and lowered thermal lensing which was evidenced in the higher output power of the laser operating with dual spectral lines at 1063/1064 nm.

In contrast to the various methods previously cited for the control of the DW power ratio, the pumping source of this DW laser was temperature-controlled. This initiative was effective enabling a variation of the pumping wavelength between 909.8 - 914.5 nm. The change in the peak wavelength of the laser diode pump was conveniently exploited for the controllability of the intensity of the either spectral line.

To the best of our knowledge, this tactic is original in its use for the purpose of tuning the power intensity ratio for a DW laser. As a direct benefit of the reduction in waste heating from the pumping technique adopted, a significant improvement in efficiency and performance was recorded with a new high in total average output power of 4.48 W from 11.55 W of absorbed power. Also, the slope and optical-to-optical efficiencies obtained were 43.8% and 38.8%, respectively. The DW laser beam had an excellent quality factor with a value of $M^2 < 1.05$ along both the horizontal and vertical directions (minimally deviating from the ideal case, $M^2 = 1$). Compared to similar DW lasers previously reported, this laser offers a simple design and a particularly simple configuration providing flexible DW operation with novel dynamic power ratio tuning. Furthermore, it delivers higher efficiency and a reduction in crystal lensing due to the decreased thermal loading thus opening a pathway for further power scaling.

Hence the results presented from this study present new areas and opportunity for future work. This may be explored towards increasing the power output from the laser. Since the output power was limited by the available pump power, further output scaling in this respect may be pursued by using a pump with a higher capacity. On the other hand, a longer crystal can be used to ensure higher pump power absorption or retro-reflection of the unabsorbed pump power back into the crystal. It is worth noting, however, that the use of a longer crystal to increase pump absorption will preclude one from designing of efficient and extremely compact (i.e. <1 mm) DW lasers based on long wavelength pumping.

To scale the output further, this laser may be investigated with more improved crystal cooling using other medium or arrangement. An attempt can be made to implement cooling on all the four sides of the crystal instead of only two that was applied in this work based on the available laser setup in the university lab. Additionally, the slope efficiency can be further increased by initiatives that ensure reduction of the intracavity losses, for instance, by utilizing a crystal with a dichroic mirror (DM) on one side and replacing the flat output coupler with a curved mirror thus having only a 2-mirror cavity instead of 3 as implemented in this work. Each highly reflecting mirror introduces unavoidable parasitic losses (observed as power leakage behind the mirror) due to coating imperfection. As another avenue, this continuous-wave DW laser may also be investigated for the possibility of operation around 1300 nm where both crystals also have distinct emission lines.

Instead of the CW operation, further investigation in the pulsed regime may be considered. In which case it could be mode-locked or Q-switched. The former involves forcing a fixed relationship on the amplitude and phase from one mode to another which causes the longitudinal modes to constructively interfere and produce a very brief (picoseconds to femtoseconds) but high intensity pulse of radiation with a wide range of potential applications. In the case of the Q-switching, the cavity gain or loss is

usually actively or passively modulated by an attenuator in such a way as to intermittently prevent light round trip in the cavity. The overall effect is the repetitive gain saturation and then near instantaneous depletion which periodically turns the lasing on and off. Q-switching produces pulsed outputs of relatively higher energies (μJ to mJ) than in the mode-locked condition (nJ) albeit at the expense of longer pulse duration (typically nanoseconds). In both cases, dramatic enhancement in peak power (from W in CW regime to kW and MW in the pulsed) can lead to significant improvement of efficiency of various nonlinear frequency conversion processes such as DFG widely used in generation of THz radiation.

References

1. W. Koechner, Solid State Laser Engineering (Springer, 2006).
2. B. M. Walsh, "Dual Wavelength Lasers," Laser Phys. 20, 622-634 (2010).
3. Y. J. Huang, H. H. Cho, Y. S. Tzeng, H. C. Liang, K. W. Su, and Y. F. Chen, "Efficient dual-wavelength diode-end-pumped laser with a diffusion-bonded Nd:YVO_4/Nd:$GdVO_4$ crystal," Opt. Mater. Express 5, 2136-2141 (2015).
4. M. Nadimi, A. Major, Continuous-wave dual-wavelength operation of a diode-pumped Nd:$GdVO_4$ laser at the 1063 & 1071 nm, 1063 & 1083 nm and 1083 &1086 nm wavelength pairs. Laser Physics. 28. 095001. (2018).
5. A. J. Singh, S. K. Sharma, P. K. Mukhopadhyay, S.M. Oak, "Dual wavelength operation in diode-end-pumped hybrid vanadate laser", Pramana J. Phys. 75, 929 (2010).
6. T. Waritanant and A. Major, "Dual-wavelength operation of a diode-pumped Nd:YVO_4 laser at the 1064.1 & 1073.1 nm and 1064.1 & 1085.3 nm wavelength pairs," Applied Physics B, Vol. 124, No. 5, 87 (2018).
7. R. Akbari, H. Zhao, and A. Major, "High-power continuous-wave dual-wavelength operation of a diode-pumped Yb:KGW laser," Opt. Lett. 41, 1601-1604 (2016).
8. P. K. Gupta, and R. Khare, "Laser Physics and Technology - Proceedings of the School on Laser Physics & Technology," Indore, India (2012).
9. J. L. Ma, B. Xiong, L. Guo, P.F. Zhao, L. Zhang, X.C. Lin, J.M. Li, and Q.D. Duanmu, "Low heat and high efficiency Nd:$GdVO_4$ laser pumped by 913 nm," Laser Phys. Lett. 7 No. 8, 579–582 (2010).
10. M. Nadimi, T. Waritanant, and A. Major, "Thermal lensing in Nd:$GdVO_4$ laser with direct in-band pumping at 912 nm," Appl. Phys. B, 124, 170 (2018).

11. T. Waritanant, A. Major, "Thermal lensing in Nd:YVO_4 laser with in-band pumping at 914 nm," Appl. Phys. B 122(5), 135 (2016).
12. M. Nadimi, T. Waritanant, and A. Major, "High power and beam quality continuous-wave Nd:$GdVO_4$ laser in-band diode-pumped at 912 nm," Photon. Res. 5(4), 346-349 (2017).
13. D. Sangla, M. Castaing, F. Balembois, and P. Georges, "Highly efficient Nd:YVO_4 laser by direct in-band diode pumping at 914 nm," Opt. Lett. 34, 2159 (2009).
14. F. L. Chang et al., "Dual-central-wavelength passively mode-locked diffusion-bonded Nd:YVO_4 /Nd:$GdVO_4$ laser with a semiconductor saturable absorber mirror," Laser Phys. Lett., vol. 14, No. 8, p. 85803, Aug. 2017.
15. T. Waritanant and A. Major, "High efficiency passively mode-locked Nd:YVO_4 laser with direct in-band pumping at 914 nm," Opt. Express 24, 12851 (2016).
16. Y. J. Huang, H. H. Cho, K. W. Su, and Y. F. Chen, "Dual-Wavelength Intracavity OPO With a Diffusion-Bonded Nd:YVO_4/Nd:$GdVO_4$ Crystal," IEEE Photonics Technology Letters, vol. 28, No. 10, May 2016.
17. F. L. Chang et al., "Dual-central-wavelength passively mode-locked diffusion-bonded Nd:YVO_4 /Nd:$GdVO_4$ laser with a semiconductor saturable absorber mirror," Laser Phys. Lett., vol. 14, no. 8, p. 85803, Aug. 2017.
18. H. Liang , T. Huang , F. Chang, C. Sung, and Y. Chen "Flexibly Controlling the Power Ratio of Dual-Wavelength SESAM-Based Mode-Locked Lasers With Wedged-Bonded Nd:YVO_4/Nd:$GdVO_4$ Crystals," IEEE journal of selected topics in quantum electronics, vol . 24, No. 5, September/October 2018.
19. M. Nadimi, T. Waritanant, A. Major, "Discrete multi-wavelength tuning of a continuous wave diode-pumped Nd:$GdVO_4$ laser," Laser Phys. Lett. 15(5), 055002 (2018).

20. T. Waritanant, A. Major, "Discretely selectable multiwavelength operation of a semiconductor saturable absorber mirror mode-locked Nd:YVO_4 laser," Opt. Lett. 42, 3331-3334 (2017).
21. T. Waritanant, A. Major, "Diode-pumped Nd:YVO_4 laser with discrete multi-wavelength tunability and high efficiency," Opt. Lett. 42, 1149-1152 (2017).
22. R. C. Talukder, Md. Z. E. Halim, T. Waritanant, and A. Major, "Multiwatt continuous wave Nd:KGW laser with hot-band diode pumping," Opt. Lett. 41, 3810-3812 (2016).
23. Md. Z. E. Halim, R.C. Talukder, T. Waritanant, and A. Major, "Passive mode-locking of a Nd:KGW laser with hot band diode pumping," Laser Phys. Lett. 13(10), 105003 (2016).
24. T. Ogawa, Y. Urata, S. Wada, K. Onodera, H. Machida, H. Sagae, M. Higuchi and K. Kodaira, "Efficient laser performance of Nd:$GdVO_4$ crystals grown by the floating zone method," Opt. Lett. 28, 2333-2335 (2003).
25. H. Yu, J. Liu, H. Zhang, A. A. Kaminskii, Z. Wang and J. Wang, "Advances in vanadate laser crystals at a lasing wavelength of 1 micrometer," Laser Photonics Rev. 8, No. 6, 847–864 (2014).
26. Y. J. Huang, Y. S. Tzeng, C. Y. Tang, and Y. F. Chen, "Efficient Dual-Wavelength Synchronously Mode- Locked Picosecond Laser Operating on the $4F_{3/2} \rightarrow 4I_{11/2}$ Transition With Compactly Combined Dual Gain Media," IEEE J. Sel. Top. Quantum Electron, vol. 21, no. 1, pp. 56–62, Jan. 2015.
27. www.rezonator.orion-project.org
28. M. Nadimi, T. Waritanant, and A. Major, "Passively mode-locked high power Nd:$GdVO_4$ laser with direct in-band pumping at 912 nm," Laser Phys. Lett. 15, 15001 (2018).
29. Y. F. Chen, M. L. Ku, and K. W. Su, "High-power efficient tunable Nd:$GdVO_4$ laser at 1083 nm.," Opt. Lett. 30, 2107–2109 (2005).

30. H. Zhang, J. Liu, J. Wang, C. Wang, L. Zhu, Z. Shao, X. Meng, X. Hu, M. Jiang, and Y. T. Chow, "Characterization of the laser crystal Nd:GdVO4," J. Opt. Soc. Am. B 19, 18–27 (2002).
31. P. K. Mukhopadhyay, A. Nautiyal, P. K. Gupta, K. Ranganathan, J. George, S. K. Sharma, T. P. S. Nathan, "Experimental determination of the thermo-optic coefficient (dn /dT) and the effective stimulated emission cross-section (σe) of an a -axis cut 1.-at. % doped Nd:$GdVO_4$ crystal at 1.06 μm wavelength," Appl. Phys. B 77, 81–87 (2003).
32. T. Omatsu, M. Okida, A. Lee and H. M. Pask, "Thermal lensing in a diode-end-pumped continuous-wave self-Raman Nd-doped GdVO4 laser," Appl. Phys. B 108, 73-79 (2012).
33. H. Kogelnik and T. Li, "Laser beams and resonators", Appl. Opt. 5 (10), 1550 (1966).
34. P. A. Bélanger, "Beam propagation and the ABCD ray matrices", Opt. Lett. 16 (4), 196 (1991).

Appendix A – Gaussian Beams and the ABCD Law

Since the traverse electric field of laser beams approximate a Gaussian profile as they travel, a Gaussian function may be used to define a freely propagating laser beam.

$$E(r,z) = E_0\left(\frac{w_0}{w(z)}\right)\exp\left(-\frac{r^2}{w(z)^2)}\right)\exp(-i\left[kz - \tan^{-1}\frac{Z}{Z_R} + \frac{kr^2}{2R(z)}\right]) \quad \text{(A1.10)}$$

In the equation above, E_0 represents amplitude or intensity, the Rayleigh range which is the distance over the beam size increases by a factor of $\sqrt{2}$ is represented by Z_R and it is evaluated by computing $\frac{\pi w_0^2}{\lambda}$; k is the wave number as determined by $2\pi/\lambda$, $R(z)$ is the radius of curvature for the propagating wavefront.

The radius of such a beam propagating in the z direction referenced from the waist expands according to:

$$w(z) = w_o\sqrt{1 + \left(\frac{zM^2}{z_o}\right)} \quad \text{(A 1.20)}$$

Where,

z = distance from waist position

z_o = Rayleigh range otherwise the distance over the beam increases by a factor of about 2

w_o = the beam waist size at the plane where z is zero

M^2 = beam quality factor

Using the ABCD law, it is possible to predict the transformation of such a Gaussian beam leaving an optical element [33]. This prediction is done with a 2 x 2 ABCD matrix in conjunction with the entry

parameters of the beam [1, 26]. Fortunately, this law that was initially used for ray tracing, not only applies to independent optical elements but it can also be applied to multi-element optical systems just like those of the optical cavities used for a laser.

For such systems, using the entry parameters of the beam and the effective transfer function of the optical system, the exiting beam can predicted. The transfer function refers to the effective ABCD matrix representation of the entire system [33, 34]. The independent transfer matrix for each of the optical elements in the cavity may be represented as follows:

Curved mirror = $\begin{bmatrix} 1 & 0 \\ -2/R & 1 \end{bmatrix}$ Flat mirror = $\begin{bmatrix} 1 & 0 \\ 0 & 1 \end{bmatrix}$

Dielectric or crystal = $\begin{bmatrix} 1 & D/n \\ 0 & 1 \end{bmatrix}$ Free space = $\begin{bmatrix} 1 & L \\ 0 & 1 \end{bmatrix}$

Thin lens = $\begin{bmatrix} 1 & 0 \\ -1/f & 1 \end{bmatrix}$

Where, R = radius of curvature of the curved mirror

D = crystal length

n = refractive index of crystal

L = propagation distance in free space between the optical elements

f = focal length

For a beam travelling through a distance L1 in free space, the ABCD matrix is:

$\begin{bmatrix} A & B \\ C & D \end{bmatrix} = \begin{bmatrix} 1 & \mathrm{L1} \\ 0 & 1 \end{bmatrix}$

For an optical system comprising of multiple elements, the effective transfer function is derived by computing the ordered product of the independent 2 x 2 matrices representing the respective optical elements starting and ending at the same optical element. This is essentially according to how they are encountered along the path of the propagating beam.

The beam transformation can be described in terms of a complex parameter q, which incorporates beam-specific information such as the beam radius and radius of curvature, thus describes the state of the beam along its propagation direction [30, 31].

It may be evaluated as:

$$\frac{1}{q} = \frac{1}{R} - i\frac{\lambda}{\pi w^2} \qquad \text{(A 1.30)}$$

Where R = radius of curvature and w = radius of the corresponding wavefronts for propagating beam along the z- direction.

In the same way an ideal thin lens of focal length *f* transforms an incoming spherical wave to radius R2 after the lens from the radius R1 before it, yielding the relationship:

$$\frac{1}{R2} = \frac{1}{R1} - \frac{1}{f} \qquad \text{(A1.31)}$$

The phase fronts of the beam undergoes similar transformation as would a spherical wave. Since the beam diameter just before and immediately after the lens are equal, the q-parameters of a propagating beam before and after the lens are similarly related by:

$$\frac{1}{q_2} = \frac{1}{q_1} - \frac{1}{f} \qquad \text{(A1.32)}$$

Taking into account the distance or separation between them respectively with regard to the lens, where d1 and d2 correspond to the distance before and after the lens (as measure from the lens).

$$q_2 = \frac{\left(1-\frac{d2}{f}\right)q_1+(d1+d2-\frac{d1d2}{f})}{-\left(\frac{1}{f}\right)q_1+(1-\frac{d1}{f})} \quad \text{(A1.33)}$$

In terms of the ABCD law, the q parameter of the beam is transformed according to the generalized bilinear relationship expressed as:

$$q_2 = \frac{Aq_1+B}{Cq_1+D} \quad \text{(A 1.34)}$$

Also, since the beam is replicated after each cavity roundtrip, then:

$$q_2 = q_1 = \frac{Aq_1+B}{Cq_1+D} \quad \text{(A 1.35)}$$

$$= \frac{1}{q_1} = \frac{D-A}{2B} \pm i\frac{\sqrt{(1-(D+A)^2/4}}{B} \quad \text{(A1.36)}$$

Following through from equation in (A 1.3), the beam radius w^2 and the radius of curvature of the wavefront R may be evaluated as:

$$w^2 = \frac{\lambda\frac{|B|}{\pi}}{\sqrt{1-\left(\frac{\mathrm{D+A}}{2}\right)^2}} \quad \text{(A 1.37)}$$

$$\mathrm{R} = \frac{2B}{D-A} \quad \text{(A 1.38)}$$

As highlighted earlier, a stable cavity is a pre-requisite for the propagating beam to continue replicating itself after each roundtrip. Thus, from equation A 1.37 above, considering real and positive values for the beam radius w, the stability conditions or boundaries can be established for the laser cavity as:

$$-1 \leq \left[\frac{D+A}{2}\right] \leq 1, \qquad \left|\frac{\mathrm{D}+\mathrm{A}}{2}\right| < 1$$